Separation and Purification Technology 377 (2025) 134177

Contents lists available at ScienceDirect

Separation and Purification Technology

journal homepage: www.elsevier.com/locate/seppur

Experimental determination and model-based prediction of flooding points in a pilot-scale continuous liquid-liquid gravity separator

Song Zhai [a,*], Niklas Bartkowiak [a], Stepan Sibirtsev [a], Andreas Jupke [a,b,*]

[a] Fluid Process Engineering (AVT.FVT), RWTH Aachen University, 52074 Aachen, Germany
[b] Institute for Bio- and Geosciences (IBG-2), Forschungszentrum Jülich GmbH, 52428 Jülich, Germany

ARTICLE INFO

Editor: Luo Guangsheng

Keywords:
Phase separation
Continuous gravity settler
Coalescence
Dense-packed zone
Temperature
Online measurement
Dispersion

ABSTRACT

Liquid-liquid gravity phase separation is crucial in chemical, biotechnological, metallurgical, and recycling processes. However, fluctuations in the feed stream conditions of the separator significantly affect the coalescence of dispersed drops, leading to the accumulation of a dense-packed zone (DPZ) and flooding. In this study, we investigate the relationship between feed stream conditions, such as temperature, and flooding points in a pilot-scale DN200 liquid–liquid gravity separator. A temperature-controlled experimental setup enabling a temperature range of 20°C to 50 °C was constructed with artificial-intelligence-assisted online measurements of separation curves, drop size distributions, and DPZ heights. Experiments were conducted with 1-octanol dispersed in water at dispersed phase fractions of 0.3 and 0.5. Experimental data show that temperature-dependent coalescence parameters, Sauter mean diameter d_{32}, and phase fraction primarily influence flooding points. Further, we evaluated the prediction accuracy and consistency of two models from the literature, a lumped zero-dimensional model and the established Henschke model, which require solely feed stream data, geometry data, and physical properties. Both models underestimate experimental flooding points by a mean absolute percentage error and relative standard deviation MAPE ± RSD of (21.5 ± 12.2) % and (24.8 ± 14.8) % for the Henschke and 0D model, respectively. Considering the experimental relative standard error of 8.2 % accounting for 95 % confidence, the prediction accuracy and consistency of both models are reasonable. This study suggests batch settling experiments and endoscope measurements in the feed stream of the liquid–liquid separator to predict its flooding point due to fluctuations in the feed.

1. Introduction

Liquid-liquid horizontal gravity phase separators are essential unit operations in many industrial processes, including fermentation, metal extraction, and chemical manufacturing. These separators are designed to split an inflowing dispersion into its coherent phases under the influence of gravity. The dispersion is typically characterized by key parameters such as the phase fraction of the dispersed phase, drop size distribution, volumetric flow rate, temperature, and properties of the material system, such as densities, viscosities, and interfacial tension. Despite their widespread use, the efficiency and stability of liquid–liquid separators are often compromised by fluctuations in the feed stream properties, such as variations in salt concentration or temperature. In coalescence-limited phase separation systems, these fluctuations impact the coalescence behavior of dispersed drops, forming a dense-packed zone (DPZ) and, in severe cases, flooding the separator with the accumulated DPZ phase [1]. Flooding disrupts the separation process, resulting in operational shutdowns and significant economic losses. Consequently, accurately predicting the DPZ height where flooding occurs and its dynamics and preventing it are critical for ensuring stable operation.

The influence of temperature on coalescence and thus flooding is not apparent because the material system's properties affecting coalescence also change with temperature. Nevertheless, Jeffreys and Davies [2] reported a higher coalescence rate with increasing temperature. Charles and Mason [3] found that increasing temperature reduces the stability of drops resting at a flat liquid–liquid interface. The positive effect of temperature on coalescence is explained by the increase in Brownian motion that favours film rupture between two coalescing drops. Sibirtsev et al. [4] found a faster batch phase separation with increasing temperature for 1-octanol in water. Ye et al. [5] stated that the temperature has an insignificant influence on the coalescence parameter in batch phase separation for paraffin oil dispersed in water. These findings

* Corresponding authors.
E-mail addresses: song.zhai@avt.rwth-aachen.de (S. Zhai), Andreas.Jupke@avt.rwth-aachen.de (A. Jupke).

https://doi.org/10.1016/j.seppur.2025.134177
Received 17 May 2025; Received in revised form 16 June 2025; Accepted 29 June 2025
Available online 30 June 2025

Nomenclature

Roman symbols

$\overline{x}_j$	[dependent] sample mean
La_{mod}	[-] modified Laplace number
d_{10}	[µm] 10 percentile of number distribution
d_{32}	[µm] Sauter mean diameter
d_{90}	[µm] 90 percentile of number distribution
D_{S}	[m] diameter of the separator
g	[m/s^2] gravity constant
h	[m] height of phases in separator
H_{cd}	[Nm] Hamaker constant
l	[m] length of separator
n	[rpm] number of revolutions
n_j	[-] size of sample
Q	[m^3/h] total volume flow
$Q_{\mathrm{aq}} = Q_{\mathrm{c}}$	[m^3/h] volume flow of the aqueous/continuous phase
Q_{c}	[m^3/h] volume flow due to coalescence
Q_{dis}	[m^3/h] volume flow of the dense-packed zone
$Q_{\mathrm{org}} = Q_{\mathrm{d}}$	[m^3/h] volume flow of the organic/dispersed phase
Q_{s}	[m^3/h] volume flow due to sedimentation
r	[m] radius of separator
r_{a}	[m] contour of channel between drops
r_{f}	[m] radius of contact area in drop-drop or drop-interface deformation
$r^*_{\mathrm{v,mod}}$	[-] modified coalescence parameter
r^*_{v}	[-] coalescence parameter
RSE_{95}	[dependent] relative standard error accounting for 95 % confidence interval
s	[-] slip parameter
s_j^2	[dependent] empirical variance
T	[°C] temperature
t	[s] time
V	[m^3] volume

Greek symbols

$\overline{\varphi}_p$	[m^3/m^3] average dispersed phase fraction in the dense-packed zone
$\Delta\rho$	[kg/m^3] density difference
ϵ	[W/kg] specific energy dissipation rate
η	[mPa s] viscosity
γ	[mN/m] interfacial tension
ρ	[kg/m^3] density
τ	[Nm] torque
φ	[m^3/m^3] dispersed phase fraction

Subscripts

0	boundary condition
aq	aqueous phase
c	continuous phase
crit	critical height at which flooding occurs
d	dispersed phase
dd	drop-drop
di	drop-interface
dis	dispersion
DPZ	dense-packed zone
experiment	experimental data
f	flooded state
in	inlet of separator
model	modeled data
org	organic phase
out	outlet of separator
p	dense-packed zone

Abbreviations

DPZ	dense-packed zone
DSD	drop size distribution
$\mathrm{Hen}_{\mathrm{b,mod}}$	batch separation model of Henschke modified by deactivating drop-drop coalescence
$\mathrm{Hen}_{\mathrm{b}}$	batch separation model of Henschke
$\mathrm{Hen}_{\mathrm{c}}$	continuous separation model of Henschke
MAE	mean absolute error
MAPE	mean absolute percentage error

suggest an ambiguous influence of temperature on coalescence in liquid–liquid phase separation that we want to investigate experimentally.

While purely predictive models are yet unable to capture coalescence phenomena [6], combining models with lab batch settling experiments is state of the art [7]. Anyhow, several experimental works dealt with continuous liquid–liquid separation and developed correlations specific to their setup. Ruiz and Padilla [8,9] developed a correlation for the DPZ height H_{DPZ} as a function of the inlet dispersed phase flow rate Q_{d}, the settling area A_{s}, as $H_{DPZ} = K\left(\frac{Q_d}{A_s}\right)^{\alpha}$ where K and α are empirical constants determined experimentally from continuous separator experiments. Thaker et al. [10] refined the model used by Padilla et al. [9] by incorporating additional factors such as inlet drop sizes, the density ratio between continuous and dispersed phases, dispersed phase fractions, and the inlet/outlet positions. This enhanced correlation demonstrated good agreement with experimental measurements and data published by Panda and Buwa [11]. All the mentioned works retrieved information about the coalescence behavior after continuous separator experiments.

Since experiments on continuous separators are costly, models relying on information from batch settling experiments are desired. Jeelani and Hartland [12,13,14], Hartland and Jeelani [15] utilized such preliminary batch settling experiments and examined how various operational parameters, including inlet flow rates, dispersed phase fractions, and drop sizes affect the DPZ height within a separator. The Henschke model [16] is currently considered the state-of-the-art approach to designing liquid–liquid gravity separators based on information from batch settling experiments [17]. Its advantage lies in the depth of modeled physical phenomena, including drop deformation and pressure loss in the DPZ. The model shows good agreement with experimental DPZ heights for various chemical systems for both dispersion directions of the organic phase. The organic chemical systems were investigated with water: n-butanol, n-butylacetate, cyclohexane, methyl isobutyl ketone, n-hexane, and toluene. Ye et al. [5,18,19] investigated the impact of volume flow rate, disperse phase fraction, temperature, and Sauter mean diameter on the shape of the DPZ, separation efficiency, and Sauter mean diameter at the outlet of the continuous phase. Their evaluation of batch settling experiments shows that temperature does not influence the coalescence parameter for paraffin oil in water dispersions. While all the above-mentioned work investigated several aspects of continuous liquid–liquid phase separation and developed sophisticated steady-state models for the DPZ height, information on the dynamic behavior of the DPZ height remains open.

In contrast to steady-state models, dynamic models of the DPZ height give information on the dynamic evolution of the DPZ height until the DPZ phase floods the separator. Backi and Skogestad [20], Backi et al. [21,22] developed a zero-dimensional (0D) dynamic three-phase separator model for controller design to regulate the DPZ height. Nevertheless, their examples are based on in silico experiments, leaving the question of experimental applicability open. Assar et al. [23,24] extended the model from Backi et al. [21] by a population balance of the

dispersed drops in the turbulent inlet section and separation section. They were able to validate their model with steady-state experimental separation efficiencies. Velioglu et al. [25] modified the model from Backi et al. [21] by allowing only dispersed organic phase and modifying the coalescence rate based on Henschke [16]. Song et al. [26] proposed a dynamic three-phase separator model, including validation with field data, but their experiments did not include a DPZ, which is vital in coalescence-limited phase separation. Uhl et al. [27] successfully included a distributed plug flow model for a horizontal continuous liquid–liquid separator, including the DPZ, in a biological manufacturing case study. However, neither of the studies reported in the literature has investigated the prediction of the temperature-dependent coalescence rate and thus flooding points in a continuous liquid–liquid separator based on batch-settling experiments in the feed stream. To the best of our knowledge, this relationship has never been investigated, although it plays a crucial role in operating liquid–liquid separators with varying feed temperatures.

We conducted flooding experiments in a continuous liquid–liquid separator from ambient temperature up to 50 °C for 1-octanol in water to validate the 0D model described in Velioglu et al. [25]. To this end, a temperature-controlled pilot-scale experimental setup with a DN200 gravity separator was constructed and is described in Section 2. The Henschke model [16] is also evaluated to compare the model's accuracy with the 0D model. Both models are parameterized by the feed information of the separator to predict its DPZ height and thus flooding. Modeling approaches and the parameterization strategy of the Henschke and 0D model are presented in Section 3. Experimental results are verified and discussed in Sections 4.1 to 4.3. Experimental model validation was analyzed in Section 4.4. Conclusions about potential model improvements and future work are given in Section 5.

2. Experimental setup

2.1. Materials

1-octanol (99 %, Häberle Labortechnik GmbH & Co. KG) and water (100 mmol L^{-1} NaCl) were examined in the plant. Concentrations of 50 mmol L^{-1} NaCl and above did not show any influence on the phase separation in preliminary batch experiments [28]. Therefore, a concentration of (100 mmol L^{-1} NaCl) was chosen for the plant experiments. After both phases had been saturated in the plant, all the physical properties were determined from plant samples. The densities and viscosities were measured in the DMA 4100 M (Anton Paar GmbH). The interfacial tension was measured in the spinning drop tensiometer SVT20-1 (DataPhysics Instruments GmbH). In the observed temperature range, measured interfacial tensions lay within the measurement error of ±0.1 mN m^{-1}. All physical properties are summarized in Table 1.

2.2. Pilot-scale DN200 liquid–liquid separator setup

Experiments in the plant were conducted in a DN200 separator with 1.8 m length. The effective length for phase separation was reduced by a stainless steel circular plate inserted through the end nozzle of the separator. The circular plate has two orifices at the top and bottom, allowing the passing of the continuous phases. All experiments were conducted in a separator with an effective length of 1.0 m. The dispersion is generated in the continuous stirred tank (R1). The continuous stirred tank (R1) has a lab stirrer (SIR03) with torque measurement and baffles. R1 has a diameter of 115 mm and height of 187 mm. The lab stirrer is equipped with two Rushton turbines with an outer diameter of 44.8 mm and a spacing of 35 mm. Temperature is controlled by flow heaters (W12, W22) and coil heat exchangers connected to cooling water. Batch settling experiments are conducted online in cell F2, which can be manually closed by two quick-closing pneumatic valves. The batch-settling cell has an inner diameter of 50 mm and height of 280 mm leading to a volume of 0.55 L. Smaller batch settling cells were reported in the literature suited for phase separation characterization [29]. The inlet and outlet streams of the separator are complemented by storage vessels, measurement devices, heaters, and pumps, as shown in Fig. 1. All parts are either borosilicate glass, PTFE, FFKM, or stainless steel. A complete list of used apparatuses and measurement devices is shown in the supplementary material (SM-A).

Table 1
Physical properties of the saturated biphasic plant system.

T/°C	ρ_{aq} /kg m^{-3}	ρ_{org}/kg m^{-3}	η_{aq}/mPa s	η_{org}/mPa s	γ/mN m^{-1}
20	1002.7	832.5	1.0185	8.7365	8.22
30	1000.0	825.4	0.8187	6.0428	8.22
40	996.5	818.2	0.6749	4.3628	8.22
50	992.3	810.9	0.5642	3.2303	8.22

2.3. Optical drop size and dense-packed zone analysis

The drop size distribution (DSD) at the inlet of the separator (QIRC01) is measured in real-time by fast processing of images with the neural-networkbased YOLO software [30,31,32] recorded by an endoscope. The endoscope was installed perpendicular to the flow to avoid sticking drops at the lens. Observed drop diameters are in between 280 μm to 1700 μm while the potential detection range is from 100 μm to 4000 μm. At least 2000 drops were counted for each measurement of the minimal d_{10}, Sauter mean d_{32}, and maximal diameter d_{90} as this amount was found to be sufficient to represent the DSD [33]. d_{10} and d_{90} represent the 10 % and 90 % percentile of the DSD and thus provide information about the spread and skewness of the DSD. YOLOv8n (YOLO) was chosen because its accuracy is sufficient, and its computation speed is the highest among larger models. We manually labeled over 3000 drops for training, validation, and testing of YOLO with a 70/20/10 split [34,35,36]. The error in predicting the test data of d_{10}, d_{32} and d_{90} is 4.93 %, 3.36 % and 4.20 %, respectively. A processed endoscope image is shown in Fig. 2a.

Four external cameras optically assessed the DPZ height along the continuous separator F1 (QIR03-05), and one external camera assessed the separation curves in the batch settling cell F2 (QR02). LED panels were installed for illumination, and tapelines were fixed on the glass wall for calibration. Separate YOLOv8s models were trained for the batch and continuous separator. In both models, two classes were defined: DPZ and clear phase separation. 100 and 500 images were manually labeled for the batch settling cell and continuous separator, respectively. Images were split in the 70/20/10 for training, validation, and testing. The error in predicting the test data in DPZ height for the continuous separator and separation curves for the batch settling cell are below 10 %. Images were recorded every three seconds. In Fig. 2b, the detected DPZ in the batch settling cell with its confidence is shown. A processed image in F1 is shown in Fig. 2c where blue is the upper contour and red is the lower contour of the DPZ.

2.4. Design of experiments

The design of experiments for the mixing, batch settling, and flooding studies was chosen to be full factorial. The following properties were varied: total volume flow rates Q, dispersed phase fraction $\varphi = Q_{org}/(Q_{org} + Q_{aq})$, number of revolutions in R1 n and temperature T. In all experiments, the organic phase was dispersed. Mixing investigations were conducted at $Q = 1 m^3 h^{-1}$, φ of 0.3 and 0.5, n of 0 rpm, 600 rpm, 1200 rpm and 1800 rpm, and T of 23°C, 30°C, 40 °C and 50 °C. At each point, the drop size distribution was measured at QIRC01 and the torque τ at the stirrer R1. The resulting specific energy dissipation rate ϵ [37] was then calculated as

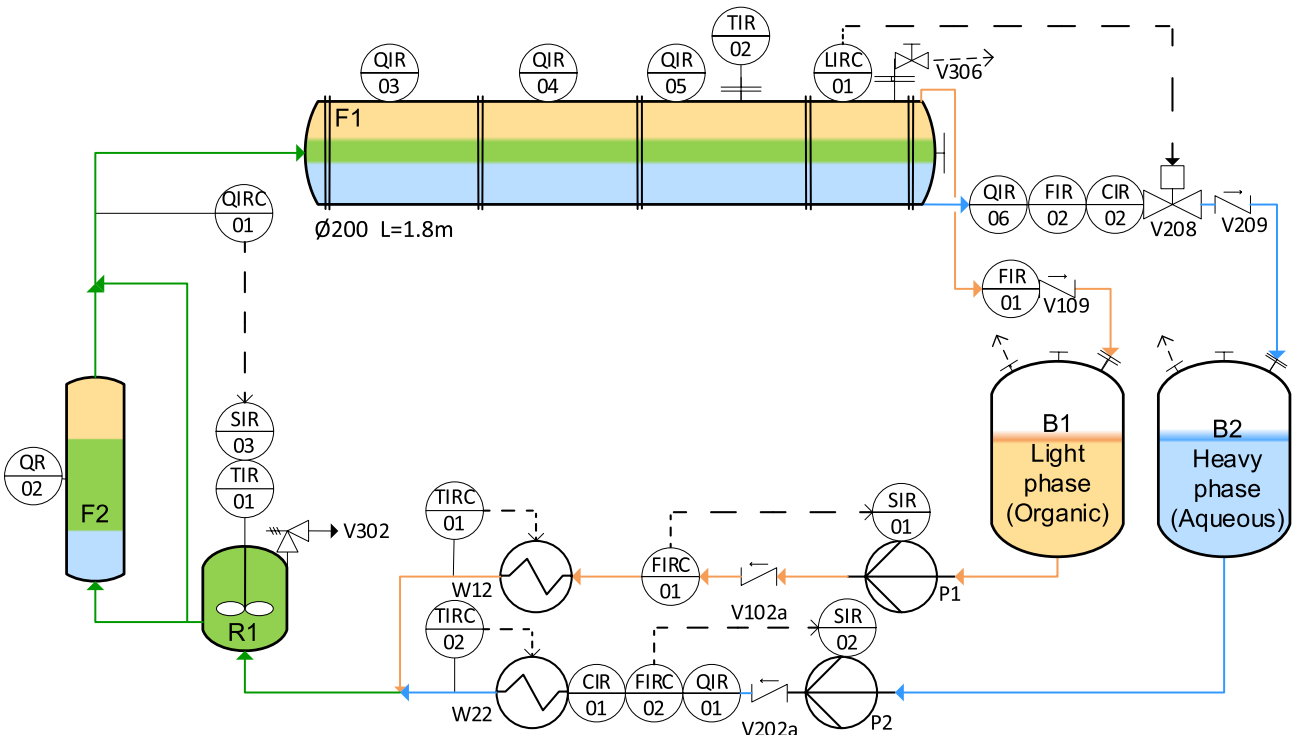

Fig. 1. Piping and instrumentation diagram of the experimental setup with DN 200 separator in the AVT.FVT lab. Blue, orange, and green colors mark the aqueous, organic, and dispersion phases. (For interpretation of the references to colour in this figure legend, the reader is referred to the web version of this article.)

$$\epsilon = \frac{2\pi n\tau}{(\rho_{\mathrm{org}} + (1-\varphi)\Delta\rho)V_{\mathrm{R1}}} \tag{1}$$

Batch settling experiments were carried out to determine the coalescence parameter r_{v}^{*}. As r_{v}^{*} is independent of Q, φ, initial Sauter diameter, and height of the batch settling cell [16], we conducted the batch settling experiments at $Q = 1\ \mathrm{m^3\,h^{-1}}$, $\varphi = 0.5$, and $n = 600$ rpm at the following temperatures: 23 °C, 30 °C, 40 °C and 50 °C.

Flooding experiments in the continuous separator (F1) were investigated at φ of 0.3 and 0.5, n of 0 rpm and 1800 rpm, and T of 23 °C, 30 °C, 40 °C and 50 °C. The inlet volume flow Q was iteratively increased until the aqueous film in the DPZ was entrained in the continuous organic phase outlet. In the experiments, both phases were cycled at least ten times the theoretical residence time until measurements were conducted to ensure homogeneity in the plant. Recorded data refer to steady-state conditions when the time-averaged Sauter mean diameter, height of DPZ, and outlet turbidity remained smaller than their measurement error for at least twice the theoretical residence time. All measurements were conducted in triplicate by reaching the operating conditions three times without shutting down the plant. Error bars indicating the 95 % confidence interval that are defined as:

$$\left[\bar{x}_j - 1.96\frac{s_j}{\sqrt{n_j}}, \bar{x}_j + 1.96\frac{s_j}{\sqrt{n_j}}\right] \tag{2}$$

where $\bar{x}_j$, s_j, and n_j are the triplicate mean, empirical variance with Bessel's correction, and number of experiments ($n_j = 3$), respectively. The relative error accounting for 95 % confidence interval RSE_{95} is defined as:

$$RSE_{95} = \frac{1.96 s_j}{\bar{x}_j\sqrt{n_j}} \tag{3}$$

3. Model-based flooding point prediction

We define flooding points as the volume flow Q entering the separator at which a significant amount of dispersed phase leaves the separator. In this work, we investigated flooding due to the accumulated DPZ phase. The DPZ height reaches a critical height $h_{\mathrm{DPZ,crit}}$ so that the aqueous film between droplets is entrained in the continuous organic phase instead of flowing through the DPZ. Therefore, flooding points are predicted by predicting Q so that the DPZ height reaches that critical height. In the following, the Henschke model for the continuous separator design ($\mathrm{Hen_c}$) is briefly shown [16]. In contrast to $\mathrm{Hen_c}$, the 0D model described in [25] captures fewer physical phenomena but is, in principle, capable of predicting the DPZ height and thus flooding. Finally, the parametrization procedure of the coalescence models used in $\mathrm{Hen_c}$ and 0D models is shown based on the batch-settling experiment. The scope of this work is to first validate both models on steady-state flooding data and conclude improvements for the 0D model. Future work deals with modeling DPZ trajectories.

3.1. Henschke model for continuous separation

In the Henschke model [16], the DPZ height h_{p}, Sauter mean diameter along the DPZ height d_{32}, and volume flow of the dispersion Q_{dis} are iteratively solved along the axial position l for given process inputs and geometry determining their boundary conditions until Q_{dis} at the separator end is zero. As boundary conditions, complete sedimentation and no coalescence are assumed after a turbulent inlet length L_{in}. Flooding points Q_{f} are calculated by finding Q so that the maximum height of the DPZ reaches the critical DPZ height $h_{\mathrm{p,crit}}$. A simplified sketch of the Henschke model is depicted in Fig. 3 that shows the main ideas of the Henschke model: Ordinary differential equations for h_{p}, Q_{dis}, and d_{32} that involve fluid dynamic phenomena such as pressure loss in the DPZ, wettability and coalescence phenomena in the DPZ such as drop deformation and asymmetric film drainage. The change of Q_{dis} along axial length dl is modeled as:

$$\frac{\mathrm{d}Q_{\mathrm{dis}}}{\mathrm{d}l} = \frac{8\varphi_{\mathrm{di}}D_{\mathrm{s}}d_{32,\mathrm{di}}}{3\overline{\varphi}_{\mathrm{p}}}\frac{\sigma^{5/6}H_{\mathrm{cd}}^{1/6}r_{\mathrm{f,di}}}{(6\pi)^{7/6}\eta_{\mathrm{c}}r_{\mathrm{a}}^{7/3}}r_{\mathrm{v}}^{*} \tag{4}$$

with the Hamaker constant $H_{\mathrm{cd}} = 1 \times 10^{-20}$ Nm, and phase fraction at

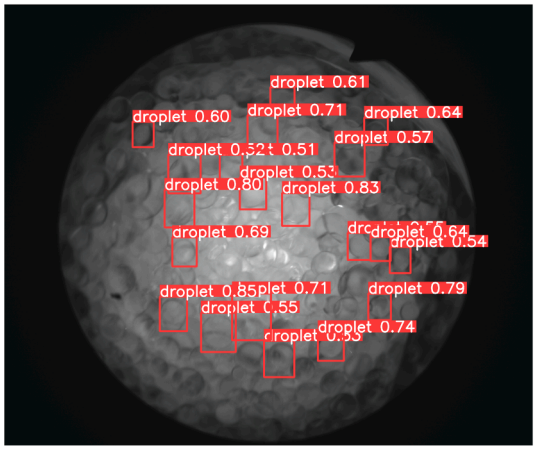

(a) Detected drops labeled with their detection confidence at QIRC01.

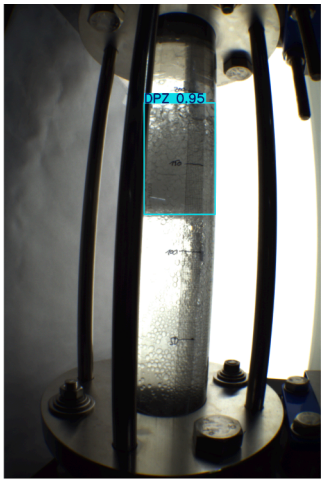

(b) Detected dense-packed zone labeled with their detection confidence at batch settling cell F2.

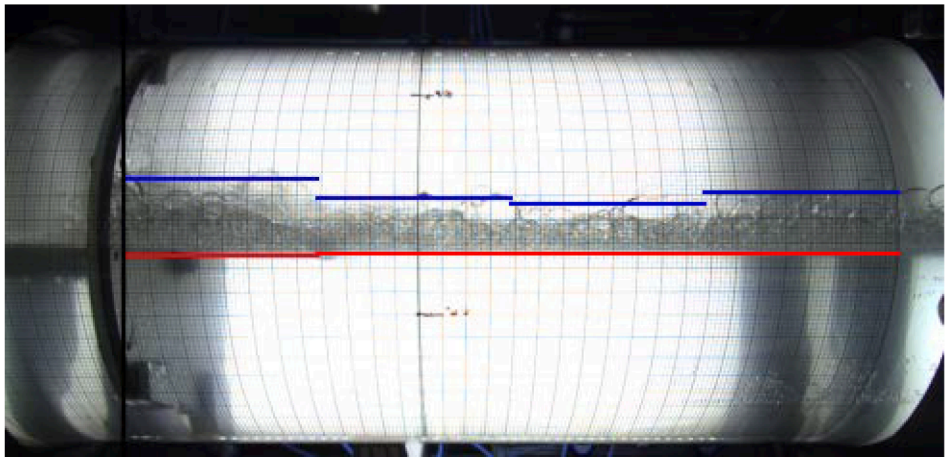

(c) Detected dense-packed zone labeled with their detection confidence at continuous separator F1, QIR04.

Fig. 2. Processed endoscope image at QIRC01 (a), processed snapshot of batch separation at QR02 (b), and camera image at QIR04 (c) to measure the drop size distribution and height of the dense-packed zone. Images are taken at temperature T = 40 °C. YOLOv8n is used to detect the drops. Separation curves are detected by YOLOv8s and manually corrected by the attached scale outside the glass. The dense-packed zone in the separator is processed with YOLOv8s.

the interface $\varphi_{di} = 1$. $d_{32,di}$ is the Sauter mean diameter at the interface, $r_{f,di}$ the radius of contact area in drop-interface deformation, r_a the contour of channel between drops, and r_v* the dimensionless coalescence fitting parameter. The parameterization of the coalescence model by the coalescence parameter r_v* is discussed in Section 3.3. The complete model and boundary conditions are shown in the supplementary material (SM-B). The numerical parameters, such as the number of discretizations and termination criteria, can be found in Henschke [16].

3.2. Zero-dimensional model for continuous separation

The 0D model balances the volume of the aqueous phase, DPZ, and organic phase as shown in Fig. 4. By transforming the volumes to heights for the cylindrical separator with radius r and length L, the following ordinary differential equations are obtained:

$$\frac{dh_{org}}{dt} = \frac{Q_{in} - Q_{aq,out} - Q_{org,out}}{2L\sqrt{h_{org}(2r - h_{org})}} \tag{5a}$$

$$\frac{dh_{DPZ}}{dt} = \frac{Q_{in} - Q_{aq,out} - Q_c}{2L\sqrt{h_{DPZ}(2r - h_{DPZ})}} \tag{5b}$$

$$\frac{dh_{aq}}{dt} = \frac{Q_{in} - Q_{aq,out} - Q_s\frac{1}{\bar{\varphi}_p} + Q_c\frac{1-\bar{\varphi}_p}{\bar{\varphi}_p}}{2L\sqrt{h_{aq}(2r - h_{aq})}} \tag{5c}$$

with h_{org}, h_{DPZ}, and h_{aq} as the heights of the organic, the DPZ, and the aqueous phase, respectively. The constitutive equations for the sedimentation rate Q_s accounts for swarm sedimentation of droplet classes [38] that was also applied to liquid–liquid extraction columns [32,39] and has the form of Stokes' law [40] for hold-ups approaching zero. Experimental outlet phase fractions of the liquid–liquid separator were confirmed by Stokes' law [5]. The coalescence rate Q_c is modeled in the same way as in the Henschke model, including drop deformation and asymmetric film drainage [16]. Compared to the Henschke model, the turbulent inlet length is indirectly modeled by swarm sedimentation. In addition, no drop-drop coalescence is considered, implying a constant Sauter mean diameter. Further, plug flow and an instantaneous formation of the flow profile without turbulence is assumed. A detailed description of the constitutive equations is found in Velioglu et al. [25]. The parameterization of this modified coalescence model by the modified coalescence parameter $r_{v,mod}$* is discussed in Section 3.3.

Flooding points are determined by assuming a constant and filled separator ($\frac{dh_{org}}{dt} = 0,\ h_{org} = h_{DPZ,crit}$) and a constant height of the aqueous

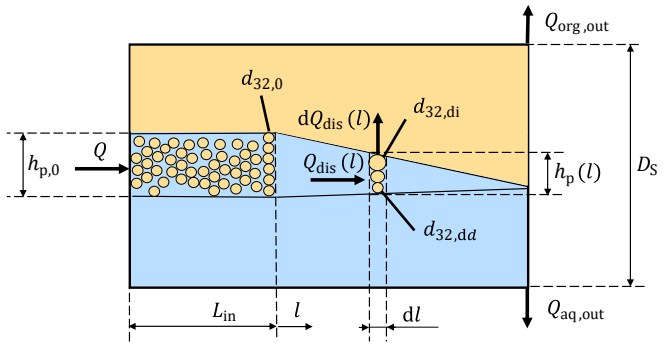

Fig. 3. Simplified sketch of the separator model by Henschke with turbulent inlet length L_{in} forming the boundary conditions for the DPZ height $h_{p,0}$. The separator has the diameter D_S with inlet volume flow Q, outlet volume flow of the organic $Q_{org,out}$ and aqueous phase $Q_{org,aq}$, and entering Sauter mean diameter of the dispersion $d_{32,0}$. At axial position l, drop-drop coalescence occurs along the height, giving the Sauter mean diameter in the DPZ $d_{32,dd}$ and at the interface $d_{32,di}$. Interfacial coalescence causes the coalesced volume flow $dQ_{dis}(l)$. The available time for coalescence is determined by the ingoing volume flow of the dispersion $Q_{dis}(l)$ and height of the DPZ $h_p(l)$. The detailed sketch and solution algorithm are in [16].

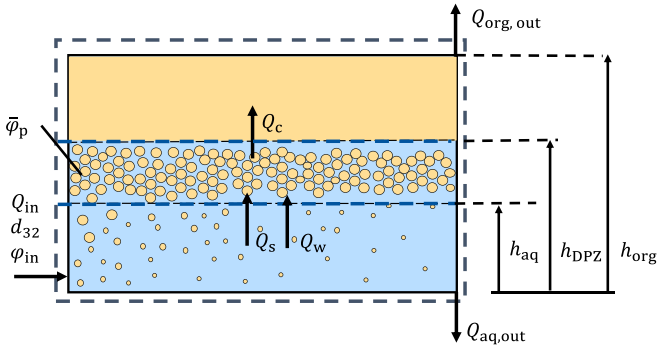

Fig. 4. Separator with the organic phase (top), dense-packed zone (center), aqueous phase (bottom), and flows. The volume flow Q_{in} enters the aqueous phase with phase fraction φ_{in} and Sauter mean diameter d_{32}. In the aqueous phase, the volume flow by sedimenting drops Q_s and entrained aqueous phase Q_w flows to the DPZ. The coalescence rate Q_c deplets the DPZ that is assumed with a constant phase fraction $\bar{\varphi}_p = 0.9$. The separator has two outgoing volume flows for each continuous phase, namely $Q_{org,out}$ and Qaq,out.

phase at the known interfacial position ($\frac{dh_{aq}}{dt} = 0,\ h_{aq} = r$). The sedimentation rate Q_s is a function of the inlet volume flow as it defines the residence time for drops to sediment. Subsequently, the outlet volume flow of the aqueous phase is entirely defined by known input variables as

$$Q_{aq,out,f} = Q_f - Q_{s,f}\frac{1}{\bar{\varphi}_p} + Q_{c,f}\frac{1-\bar{\varphi}_p}{\bar{\varphi}_p} \tag{6}$$

Inserting Eq. (6) into Eq. (5b) with $\frac{dh_{DPZ}}{dt} = 0$, we receive the following equation to determine the flooding point Q_f at a given constant critical DPZ height $h_{DPZ,crit}$.

$$0 = Q_{s,f} - Q_{c,f} \tag{7}$$

3.3. Coalescence parametrization based on batch-settling experiment

Batch-settling experiments with the same material system as in the continuous separator are used to parameterize the coalescence models for the continuous liquid–liquid separator and batch separation. The batch settling experiment is usually conducted in a stirred glass vessel with external cameras to record the separation process. Fig. 5 shows a

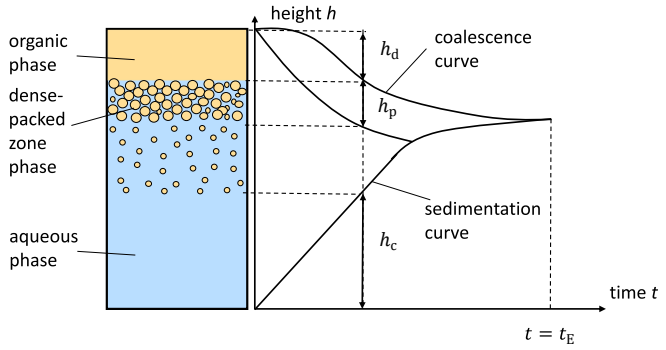

Fig. 5. Batch-settling experiment (left-hand side) and corresponding settling curve (right hand side) adapted from Henschke [17]. h_d, h_p and h_c are the heights of the dispersed phase, dense-packed zone, and continuous phase, respectively. The phase separation ends at t_E.

snapshot of the batch-settling experiment and the experimentally recorded sedimentation and coalescence curve. These curves are the basis for parameterizing the coalescence models of the investigated material system.

The batch separation model of Henschke [16,17] consists of free swarm sedimentation, drop-drop and drop-interface coalescence, and drop deformation in the DPZ. Notably, Henschke's batch (Hen_b) and continuous separation models (Hen_c) share only the same coalescence model, yet are two separate models. The experimental sedimentation curve and the swarm sedimentation model of Pilhofer and Mewes [41] with single drop sedimentation of Ishii and Zuber [42] are used to estimate the initial Sauter mean diameter by assuming no coalescence during sedimentation. With an estimated initial Sauter mean diameter, the formation of the DPZ by swarm sedimentation is described. Inside the DPZ, drop-drop coalescence induced by drop deformation and hydrostatic pressure results in a growing Sauter mean diameter along the height. Drop-interface coalescence depletes the DPZ, resulting in an experimentally trackable coalescence curve. r_v* in the drop-drop and drop-interface coalescence rate is estimated to fit the experimental coalescence curve and separation time t_E. The determined r_v*, including the drop deformation and coalescence model, is transferred to the continuous separator model to describe the coalescence-limited depletion of the DPZ.

The determination of $r_{v,mod}$* for the 0D model differs from the approach in the batch Henschke model (Hen_b) [16] since no drop-drop coalescence is assumed. Therefore, we modified the fitting procedure with the batch separation model by neglecting drop-drop coalescence in the DPZ (referred to in this work as $Hen_{b,mod}$). $r_{v,mod}$* lumps the coalescence effects of drop-drop and drop-interface into solely drop-interface coalescence. Consequently, $r_{v,mod}$* must be greater than the conventional coalescence parameter r_v*.

4. Results and discussion

This section shows the impact of temperature on the flooding point in the liquid–liquid separator. Firstly, the mixing behavior of 1-octanol in water is investigated. Subsequently, the influence of temperature on the coalescence parameter r_v* and the modified coalescence parameter $r_{v,mod}$* determined online by the batch-settling cell is discussed. Both experimental information are combined to describe the observed flooding points Q_f. Finally, the 0D and Henschke models are evaluated to predict the experimental flooding point $Q_{f,experiment}$.

4.1. Analysis of mixing in the stirred tank

Evaluating the predictive models for the continuous separator requires information about the drop size distribution (DSD) of the inflowing dispersion. Since the mixing behavior of 1-octanol in water

was reported in the literature to follow a counterintuitive trend [16], we characterized its mixing behavior in our experimental setup by endoscope measurements at QIRC01 (see Fig. 1).

Experimental investigations of 1-octanol in water revealed that the Sauter mean diameter d_{32} in stirred systems is strongly influenced by phase fraction φ, energy dissipation rate ϵ, and temperature T, as shown in Fig. 6. Higher φ leads to a larger d_{32} that can be attributed to the increased collision frequency of drops at higher φ promoting coalescence. The dominance of coalescence over breakage under these conditions results in larger drops and a higher overall d_{32}. The observed influence of φ on d_{32} aligns with experimental studies in the literature [5,43,44]. The relationship between ϵ and d_{32} exhibited a temperature-dependent behavior. At ambient T and 30°C, increasing ϵ resulted in a larger d_{32}. This counterintuitive trend suggests that the coalescence rate increases more rapidly than the breakage rate as ϵ rises. Our observation is consistent with findings reported in the literature for this material system [16]. Conversely, at 40°C and 50°C, d_{32} stagnated once the number of revolutions n exceeds 600 rpm, indicating that coalescence and breakage rate increases in the same order with ϵ. Beyond this point, additional ϵ did not alter d_{32} significantly. Further information about the d_{10} and d_{90} is shown in the supplementary material (SM-C). In summary, we observed that d_{32} predominantly depends on φ followed by T and, to a minor extent, on ϵ.

4.2. Evaluation of phase separation in the online batch-settling cell

The flooding point depends on the coalescence rate, again a function of r_v* or $r_{v,mod}$* depending on which model should be parameterized. The r_v* is fitted to separation curves retrieved from batch-settling experiments. The sedimentation and coalescence curves are depicted in Fig. 7. Since the lighter organic phase is dispersed, the sedimentation curves correspond to the bottom and the coalescence curves to the upper curves. The sedimentation curves show a roughly linear trend in the free sedimentation period, with higher T leading to decreasing slopes, indicating a slower sedimentation rate. The coalescence curves exhibit a characteristic S-shape, reflecting the dynamic nature of drop-drop and drop-interface interactions. Notably, the time required for phase separation increases with T until 40 °C after which the separation time stagnates. The Henschke batch separation model (Hen_b) were applied [16] to decouple the effects of changing physical properties, such as the continuous phase viscosity and the initial d_{32}, on coalescence rates. Applying the Hen_b model requires determining the initial d_{32}. To fit r_v* and $r_{v,mod}$*, the estimation of the initial d_{32} by the conventional sedimentation and endoscope method is compared in the following.

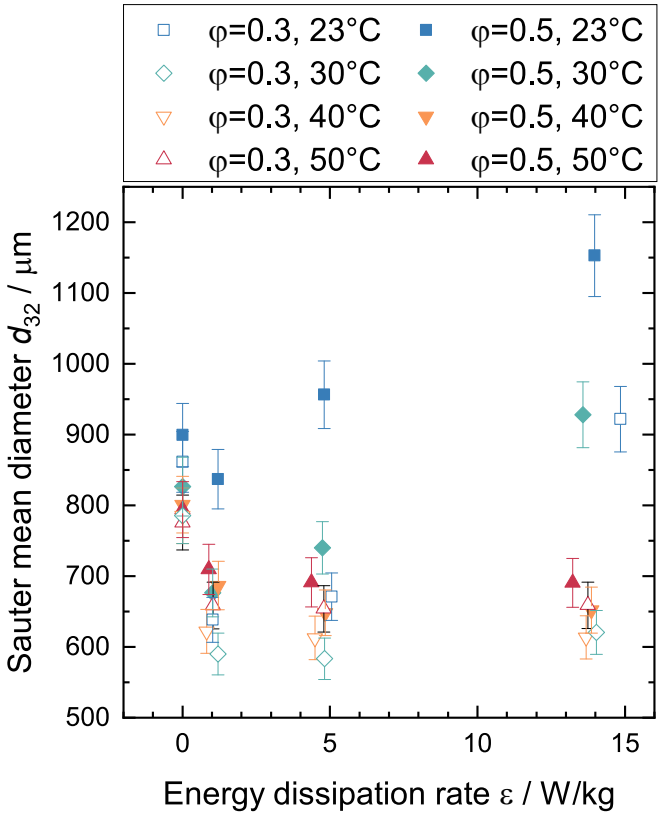

Fig. 6. Sauter mean diameter d_{32} as a function of energy dissipation rate ϵ, temperature T, and phase fraction φ. Experiments are conducted at volume flow rate $Q = 1\ m^3\ h^{-1}$. Error bars show the accuracy of the endoscope measurement and evaluation with YOLO.

The comparison of the two estimation methods for determining the initial d_{32} and, thus, the r_v* reveals notable differences under varying T conditions, as shown in Fig. 8. Fig. 8a illustrates the estimated and measured d_{32} as a function of T. The sedimentation method consistently estimated higher values than the endoscopic measurement, with the deviation becoming more pronounced at lower T, particularly at 23 °C, where higher turbidity complicates the identification of the sedimentation curve. This behavior is attributed to the turbid nature of the system at this T, which complicates accurate sedimentation curve detection as shown in the supplementary material (SM-D). A general source of error is drop-drop coalescence induced by the quick-closing valves abruptly stopping the dispersion flow. Consequently, the estimated d_{32} by the sedimentation curve must be larger than the measured values from the endoscope. A further source of deviation results from the measurement position: a transition from DN50 to DN40 piping half a meter downstream of the batch-settling cell may introduce discrepancies. For higher T, the error in the estimated values relative to the measured ones aligns with literature-reported values [16], within a range of 25 %.

The influence of d_{32} on r_v* and $r_{v,mod}$* is shown in Fig. 8b. As expected, the values determined from the modified coalescence model are higher than those from the Henschke model because a higher drop-interface coalescence fits the lack of drop-drop coalescence. At 40 °C and 50 °C, no significant difference between the estimation methods can be concluded based on the error bars, while at 30 °C, a slight deviation is observed. Since systems at the elevated T exhibited clear phase separation, the results confirm that endoscopic measurements can reliably estimate the initial d_{32} for fitting r_v* and $r_{v,mod}$* with a relative standard error accounting for 95 % confidence RSE_{95} of less than 8 % and 6 %, respectively. The resulting fit to batch separation data is shown in Fig. 7. The choice between relying on the blurred sedimentation curve or the endoscopic measurement remains critical for turbid systems. r_v* and $r_{v,mod}$* estimated by the endoscopic method exhibit a significant RSE_{95} of 82 % and 17 %, as shown in SM-D, resulting in an unreliable estimation. Using the sedimentation method, the parameterized batch Henschke model (Hen_b) and its modification ($Hen_{b,mod}$) neglecting drop-drop coalescence both agree with the experimental batch separation data, as shown in Fig. 7. In summary, the sedimentation method was used to determine r_v* and $r_{v,mod}$* because the resulting fit to batch separation data is satisfactory.

Notably, material systems with a similar r_v* value at ambient T were found for n-butanol and cyclohexanone in water with 0.0832 and 0.0798, respectively [16]. In contrast, Ye et al. [5] found no significant T influence on the r_v* for paraffin oil in water for T between 20 °C to 80 °C. Yet, they found a decreasing r_v* for water in paraffin oil. The differing trends observed here may be explained by factors such as impurities in both experimental setups. Impurities could attach to the interface of both phases to different degrees of coverage depending on the T so that the asymmetric film drainage is hindered. Nevertheless, the r_v* or $r_{v,mod}$* effectively encapsulates all such influences, enabling the modeling of the flooding point of the same material system in the continuous separator. The prediction accuracy of flooding points in the continuous separator by the Henschke and 0D dynamic model parameterized by r_v*

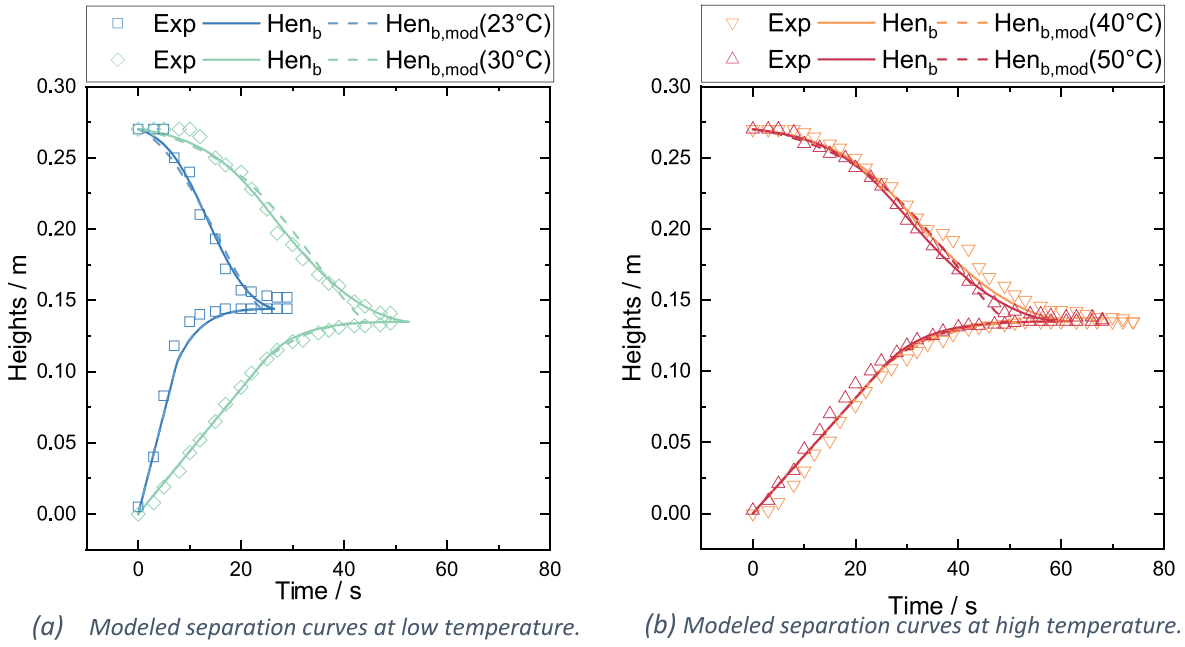

Fig. 7. Batch-settling curve from settling cell F2 at the corresponding temperatures and at Q = 1 $m^3\ h^{-1}$, φ = 0.5, and n = 600rpm. The Henschke batch model (Hen_b) [17] and the modified version ($Hen_{b,mod}$) Section 3.2 were fitted here. Both models were fitted with the sedimentation approach.

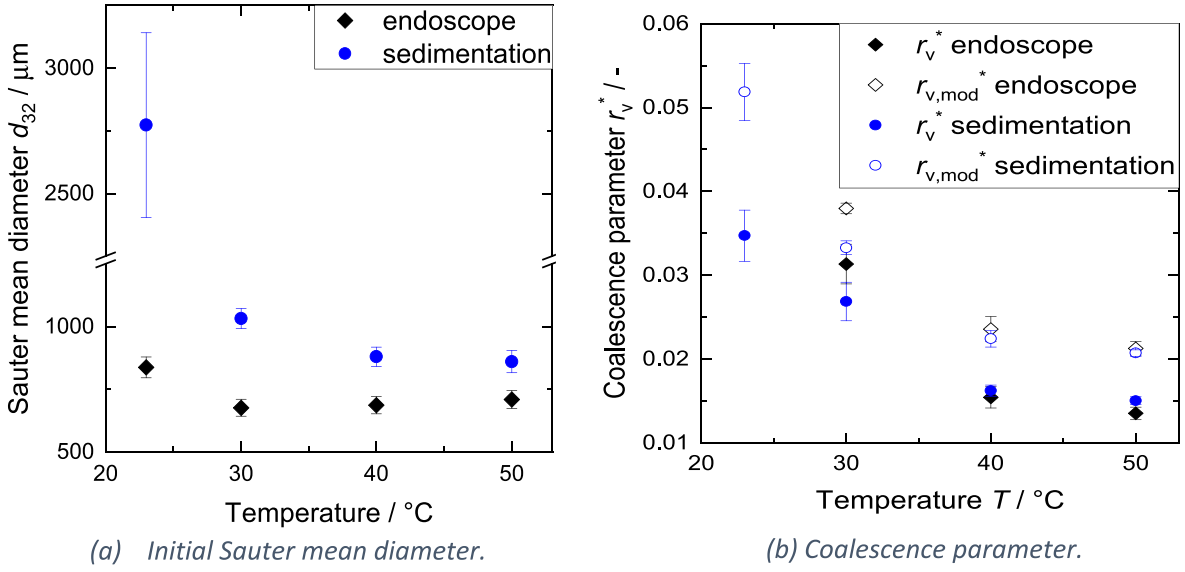

Fig. 8. Comparison of initial Sauter mean diameter determination with endoscope against conventional estimation method based on the sedimentation curve and Henschke model [17]. The influence on the coalescence parameter and modified coalescence parameter $r_{v,mod}$* is compared. Error bars show the maximum of the 95 % confidence interval and measurement accuracy. The coalescence parameter determined by the endoscope method at ambient temperature is omitted and shown in SM-D. Experiments were conducted at Q = 1m^3h^{-1}, φ = 0.5, and n = 600 rpm.

and $r_{v,mod}$*, respectively, is discussed in Section 4.4.

4.3. Characterization of experimental flooding points

The flooding point Q_f is found at the incoming volume flow resulting in an accumulation of the DPZ so that the aqueous film between drops in the DPZ are entrained and flushed out to the organic outlet. Throughout all flooding experiments, flooding was observed at a DPZ height of 30 mm. Physical properties and operating conditions influence fluid dynamics and thus flooding. Here, we investigate how physical properties in terms of changing temperature and operating conditions affect Q_f. As shown in Section 4.2, the coalescence was influenced by the operating temperature T.

The influence of T on Q_f at all φ and stirring speed is shown in Fig. 9a. At higher T, Q_f decreases, aligning with the reduction in the r_v* discussed in Section 4.2. For instance, Q_f at 50 °C and 40 °C are comparable, as the d_{32} and r_v* do not vary significantly between these T. A slightly larger Q_f is observed at 30 °C, corresponding to a higher r_v*. Q_f is consistently higher at ambient T, where the aqueous phase was turbid and the r_v* reaches its maximum. The r_v* from batch-settling experiments without knowing d_{32} can qualitatively explain the trend of T-dependent Q_f that can also be seen by the proportional relationship between coalescence rate and r_v* in Eq. (4).

The influence of operating conditions on Q_f was analyzed under

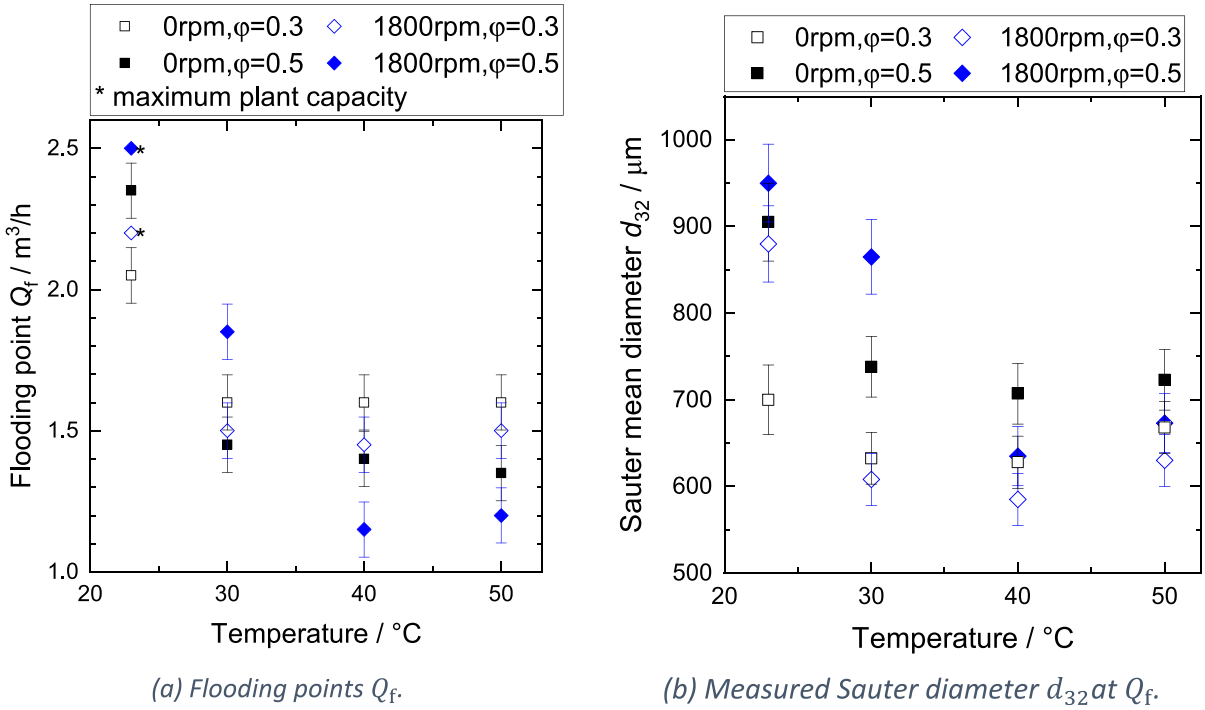

(a) Flooding points Q_f. *(b) Measured Sauter diameter d_{32} at Q_f.*

Fig. 9. Flooding points at two phase fractions and stirring speeds. The measured Sauter mean diameter (d_{32}) at QIRC01 is shown at their respective flooding point. Flooding is specified by the overflow of dense-packed zone at an effective separator length of 1 m.

varying stirring speeds and φ. An important fluid dynamic information of the system is the inflowing d_{32} since a larger d_{32} enhances the phase separation and thus increases Q_f. Therefore, in addition to Q_f, the corresponding measured d_{32} are shown in Fig. 9b. The influence of d_{32} on Q_f can be seen by comparing the two stirring speeds for each T and φ. A larger Q_f for larger d_{32} is observed for all operating points. This observation is expected, since sedimentation and coalescence rates are faster for increasing d_{32} that can be seen by Eq. (4). Operating conditions with similar d_{32} and different φ were observed for the following data points: i) at $T = 23$°C: $\varphi = 0.3$, 1800 rpm and $\varphi = 0.5$, 0 rpm, ii) at $T = 40$°C: $\varphi = 0.3$, 0 rpm and $\varphi = 0.5$, 1800 rpm and iii) at $T = 50$°C: $\varphi = 0.3$, 0 rpm and $\varphi = 0.5$, 1800 rpm. The ones with higher φ showed a smaller Q_f in all three data points, which is explained by the larger inlet stream of the dispersed phase. Overall, the experimental Q_f are explainable with φ, r_v*, and d_{32}.

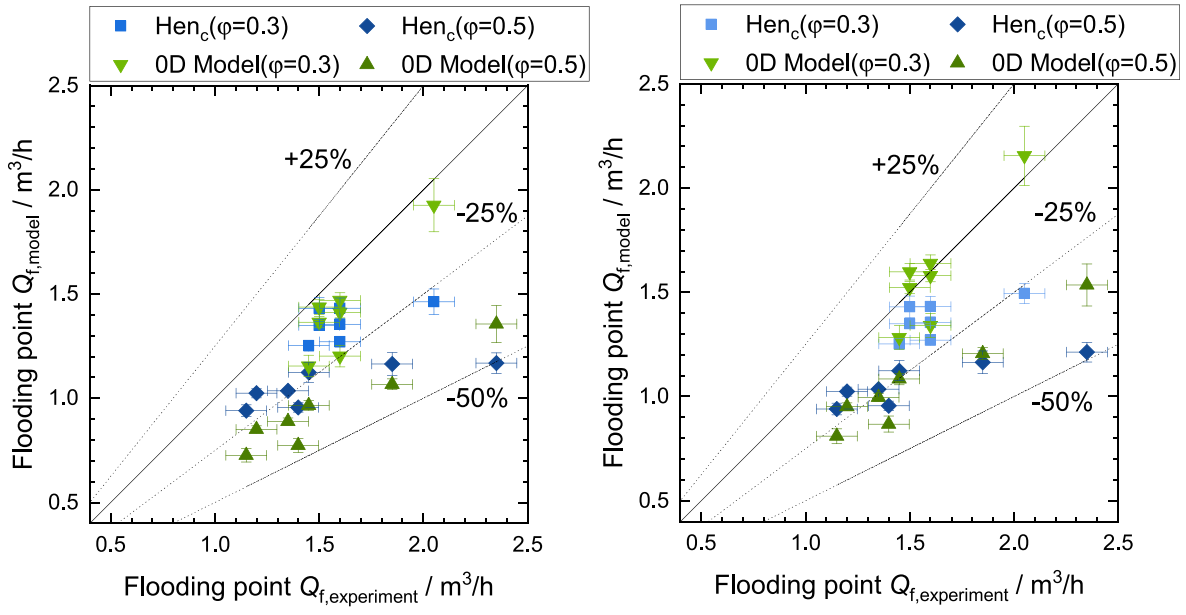

(a) Measured d_{32}. *(b) Increased 20 % of measured d_{32}.*

Fig. 10. Parity plot of modeled flooding points Q_f with the Henschke continuous model (Hen$_c$) and 0D model. Measured d_{32} is compared to an increased d_{32} of 20%. Error bars show the influence of the determined coalescence parameter and experimental triplicates with 95 % confidence interval.

4.4. Comparative validation of flooding-point prediction models

The comparative analysis of the 0D and Henschke model reveals distinct patterns in predicting Q_f with process information of the feed stream of the separator, as shown in Fig. 10a. Both models underestimate the experimental $Q_{f,experiment}$. For the 0D model, the prediction accuracy and consistency of Q_f as mean absolute percentage error (MAPE) and the relative standard deviation of errors (RSD) are classified by φ. $\varphi = 0.3$ and $\varphi = 0.5$ were underestimated by (12.0 ± 7.7)%, and (37.5 ± 5.7)%, respectively. The continuous separation model of Henschke (Hen_c) demonstrated a MAPE ± RSD of (14.8 ± 7.9)% for $\varphi = 0.3$, and (28.3 ± 12.4)% for $\varphi = 0.5$. Both models showed a poor prediction accuracy for ambient T and $\varphi = 0.5$ that might be attributed to the turbid system. The prediction accuracy is compared to the ratio of the 95 % confidence interval to its mean of 8.2 % for $\varphi = 0.3$ highly accurate, for $\varphi = 0.5$ reasonable, and in total acceptable. The mean absolute error (MAE) and corrected sample standard deviation of the prediction error s of Q_f are shown in Table 2. Both models have a similar MAE and s, meaning both models have similar prediction accuracy and consistency. In summary, the Hen_c showed a slightly better prediction accuracy and similar consistency of Q_f than the 0D model (MAPE ± RSD of (21.5 ± 12.2)% against (24.8 ± 14.8)%, MAE ± s of (0.36 ± 0.29)m^3 h^{-1} against (0.39 ± 0.27)m^3 h^{-1}).

The general underestimation of both models might be attributed to largerthan-measured d_{32} due to feed stream geometry effects, such as the influence of the one-quarter DN50 pipe between the d_{32} measurement and the separator inlet. Additionally, the r_v* fitted in batch experiments may lack transferability to continuous systems at flooding conditions because Hen_c aims to model wedge-shaped dense-packed zones (DPZs), whereas the present system exhibits band-shaped DPZs.

The actual d_{32} at the inlet of the separator is assumed to be larger than the measured values due to the residence time and coalescence in the onequarter DN50 pipe. To account for this effect, models were simulated with an increased d_{32} by 20 % to estimate drop-drop coalescence in the inlet, as shown in Fig. 10b. Q_f determined by Hen_c do not show considerable sensitivity to the inlet d_{32}, while the MAPE and RSD of the Q_f prediction of the 0D model is reduced to (18.1 ± 13.5)% indicating a slight increase in consistency and accuracy. If the onequarter DN50 pipe exhibits such a coalescence effect on the dispersion, the 0D model will have better accuracy in predicting Q_f.

Nevertheless, using the 0D model with determined $r_{v,mod}$ in the feed stream to predict Q_f in a continuous liquid–liquid separator requires measurements of the d_{32} at the inlet within 20 % accuracy.

Overall, the comparison highlights the need to refine the measurement position of the endoscope and refine the 0D model to achieve better prediction accuracy and consistency at high φ. Since both models are similar in accuracy and consistency, the direction of model refinement cannot be directly drawn and is thus a future work. Both models leverage process inputs, including volume flows, d_{32}, and batch-derived coalescence parameters, to predict Q_f under varying feed conditions. Both predictions underestimate Q_f, which means a conservative estimation for operating a continuous liquidliquid separator. Transferring the method to predict Q_f to industrial applications requires sample points in the feed stream of the separator to conduct the batch separation experiment and a d_{32} measurement at the separator inlet.

5. Conclusion and outlook

In this work, we constructed a novel experimental setup with extensive online measurements to investigate the liquid–liquid phase separation in a pilot-scale horizontal gravity separator. The artificial-intelligence-assisted online measurement of the coalescence parameter and Sauter mean diameter d_{32} allowed the experimental investigation of flooding in the separator with the dense-packed zone (DPZ). 1-Octanol dispersed in aqueous 100 mM NaCl solution was investigated. The temperature-dependent flooding points of the separator were experimentally assessed for two phase fractions and stirring speeds with a relative standard error of 8.2 %. By conducting and analyzing online batch-settling experiments, a temperature-dependent coalescence parameter was found to describe the trends in mixing and separation at their respective temperatures. In addition, the experimental flooding points were predicted with the Henschke model [16] and a comparatively simplified 0D model [25]. Both models underestimate the experimental flooding points by a mean absolute percentage error and relative standard deviation MAPE ± RSD of (21.5 ± 12.2)% against (24.8 ± 14.8)% for the Henschke and 0D model, respectively. To account for a potentially larger d_{32} at the separator inlet due to piping, a 20 % increased d_{32} results in a MAPE ± RSD of (18.1 ± 13.5)% for the 0D model while the values for the Henschke model remains the same. Considering the relative standard error of the experimental data, the prediction accuracy and consistency of both models are reasonable. Future work will extend and validate the 0D model to predict the dynamics of the DPZ in the continuous liquid–liquid separator.

Table 2
Comparison of the mean absolute error MAE and corrected sample standard deviation s across different models and phase fraction φ for flooding points.

Model	$\varphi = 0.3$		$\varphi = 0.5$		Total φ	
	MAE/ m3/h	s/ m3/h	MAE/ m3/h	s/ m3/h	MAE/ m3/h	s/ m3/h
0D model	0.19	0.12	0.59	0.23	0.39	0.27
Henschke	0.25	0.17	0.48	0.35	0.36	0.29
0D model (120 % d_{32})	0.10	0.09	0.47	0.20	0.29	0.24
Henschke (120 % d_{32})	0.25	0.16	0.47	0.34	0.36	0.28

CRediT authorship contribution statement

Song Zhai: Conceptualization, Software, Investigation, Methodology, Validation, Visualization, Writing – original draft, Writing – review & editing. **Niklas Bartkowiak:** Investigation, Data curation. **Stepan Sibirtsev:** Writing – review & editing, Supervision. **Andreas Jupke:** Supervision, Funding acquisition.

Declaration of competing interest

The authors declare that they have no known competing financial interests or personal relationships that could have appeared to influence the work reported in this paper.

Acknowledgments

This work was funded by the Deutsche Forschungsgemeinschaft (DFG, German Research Foundation) – 466656378 – within the Priority Programme “SPP 2331:Machine Learning in Chemical Engineering”. The authors thank Christian Meyer, Marius Müller, Raphaela Stettner, and Lucas Zwick (Aachener Verfahrenstechnik, Fluid Process Engineering, RWTH Aachen University) for helping to construct and commission the experimental setup. We would like to give special thanks to Janik Hense, Lukas Polte, and Lukas Thiel (Aachener Verfahrenstechnik, Fluid Process Engineering, RWTH Aachen University) for their valuable suggestions and dedicated help on the separator model and experimental setup.

Appendix A. Supplementary data

Supplementary data to this article can be found online at https://doi.org/10.1016/j.seppur.2025.134177.

Data availability

Data will be made available on request.

References

[1] J. Kamp, J. Villwock, M. Kraume, Drop coalescence in technical liquid/liquid applications: a review on experimental techniques and modeling approaches, ISSN 0167-8299, Rev. Chem. Eng. 33 (1) (2017) 1–47, https://doi.org/10.1515/revce-2015-0071.

[2] G.V. Jeffreys, G.A. Davies, Coalescence of liquid droplets and liquid dispersion, Elsevier ISBN 9780080156828, Recent Adv. Liquid-Liquid Extract. (1971) 495–584, https://doi.org/10.1016/B978-0-08-015682-8.50018-3.

[3] G.E. Charles, S.G. Mason, The coalescence of liquid drops with flat liquid/liquid interfaces, ISSN 00958522, J. Colloid Sci. 15 (3) (1960) 236–267, https://doi.org/10.1016/0095-8522(60)90026-X.

[4] S. Sibirtsev, C.B. Göbel, A. Jupke, Automation of a procedure for the experimental investigation of liquid–liquid phase separation, ISSN 0009-286X, Chem. Ing. Tech. 91 (12) (2019) 1787–1793, https://doi.org/10.1002/cite.201900162.

[5] S. Ye, L. Hohl, E. Charlafti, Z. Jin, M. Kraume, Effect of temperature on mixing and separation of stirred liquid/liquid dispersions over a wide range of dispersed phase fractions, ISSN 00092509, Chem. Eng. Sci. 274 (2023), https://doi.org/10.1016/j.ces.2023.118676.

[6] K.-H. Reissinger, J. Schröter, W. Bäcker, Möglichkeiten und probleme bei der auslegung von extraktoren, ISSN 0009-286X, Chem. Ing. Tech. 53 (8) (1981) 607–614, https://doi.org/10.1002/cite.330530805.

[7] T. Frising, C. Noïk, C. Dalmazzone, The liquid/liquid sedimentation process: from droplet coalescence to technologically enhanced water/oil emulsion gravity separators: a review, ISSN 0193-2691, J. Dispers. Sci. Technol. 27 (7) (2006) 1035–1057, https://doi.org/10.1080/01932690600767098.

[8] M.C. Ruiz, R. Padilla, Separation of liquid-liquid dispersions in a deep-layer gravity settler: Part ii. mathematical modeling of the settler, ISSN 0304386X, Hydrometall. 42 (2) (1996) 281–291, https://doi.org/10.1016/0304-386X(95)00096-Y.

[9] R. Padilla, M.C. Ruiz, W. Trujillo, Separation of liquid-liquid dispersions in a deep-layer gravity settler: Part i. experimental study of the separation process, ISSN 0304386X, Hydrometall. 42 (2) (1996) 267–279, https://doi.org/10.1016/0304-386X(95)00095-X.

[10] A.H. Thaker, M. Darekar, K.K. Singh, V.V. Buwa, Experimental investigations of liquid–liquid disengagement in a continuous gravity settler, ISSN 02638762, Chem. Eng. Res. Des. 139 (2018) 174–187, https://doi.org/10.1016/j.cherd.2018.09.031.

[11] S.K. Panda, V.V. Buwa, Effects of geometry and internals of a continuous gravity settler on liquid–liquid separation, ISSN 0888-5885, Ind. Eng. Chem. Res. 56 (46) (2017) 13929–13944, https://doi.org/10.1021/acs.iecr.7b03756.

[12] S.A.K. Jeelani, S. Hartland, Prediction of steady state dispersion height from batch settling data, ISSN 0001-1541, AIChE J 31 (5) (1985) 711–720, https://doi.org/10.1002/aic.690310503.

[13] S.A.K. Jeelani, S. Hartland, Dynamic response of gravity settlers to changes in dispersion throughput, AIChE J. 34 (2) (1988) 335–340, https://doi.org/10.1002/aic.690340220. URL https://aiche.onlinelibrary.wiley.com/doi/10.1002/aic.690340220. ISSN 0001-1541.

[14] S.A.K. Jeelani, S. Hartland, Effect of dispersion properties on the separation of batch liquid−liquid dispersions, ISSN 0888-5885, Ind. Eng. Chem. Res. 37 (2) (1998) 547–554, https://doi.org/10.1021/ie970545a.

[15] S. Hartland, S.A.K. Jeelani, Choice of model for predicting the dispersion height in liquid/liquid gravity settlers from batch settling data, ISSN 00092509, Chem. Eng. Sci. 42 (8) (1987) 1927–1938, https://doi.org/10.1016/0009-2509(87)80139-2.

[16] M. Henschke. Dimensionierung liegender Flüssig-flüssig-Abscheider anhand diskontinuierlicher Absetzversuche: Zugl.: Aachen, Techn. Hochsch., Diss., 1994, volume Nr. 379 of Fortschritt-Berichte/VDI Reihe 3, Verfahrenstechnik. VDI-Verl., Düsseldorf, als ms. gedr edition, 1995. ISBN 3-18-337903-1.

[17] M. Henschke, Determination of a coalescence parameter from batchsettling experiments, ISSN 13858947, Chem. Eng. J. 85 (2–3) (2002) 369–378, https://doi.org/10.1016/S1385-8947(01)00251-0.

[18] S. Ye, L. Hohl, M. Kraume, Impact of feeding conditions on continuous liquid-liquid gravity separation, part i: Inlet and outlet drop size, dense-packed zone and separation efficiency, ISSN 00092509, Chem. Eng. Sci. 282 (2023), https://doi.org/10.1016/j.ces.2023.119237.

[19] S. Ye, L. Hohl, M. Kraume, Impact of feeding conditions on continuous liquid-liquid gravity separation, part ii: Inlet/outlet drop size distribution and fractional separation efficiency, ISSN 00092509, Chem. Eng. Sci. 285 (2024), https://doi.org/10.1016/j.ces.2023.119611.

[20] C.J. Backi, S. Skogestad, A simple dynamic gravity separator model for separation efficiency evaluation incorporating level and pressure control, in: 2017 American Control Conference (ACC), 2017, pp. 2823–2828, https://doi.org/10.23919/ACC.2017.7963379.

[21] C.J. Backi, B.A. Grimes, S. Skogestad, A control- and estimation-oriented gravity separator model for oil and gas applications based upon first-principles, ISSN 0888-5885, Ind. Eng. Chem. Res. 57 (21) (2018) 7201–7217, https://doi.org/10.1021/acs.iecr.7b04297.

[22] C.J. Backi, S. Emebu, S. Skogestad, B.A. Grimes, A simple modeling approach to control emulsion layers in gravity separators, in: 29th European Symposium on Computer Aided Process Engineering, volume 46 of Computer Aided Chemical Engineering, Elsevier, 2019, pp. 1159–1164, doi: 10.1016/B978-0-12-818634-3.50194-6.

[23] M. Assar, S. Simon, G.H. Sørland, B.A. Grimes, A theoretical and experimental investigation of batch oil-water gravity separation, ISSN 02638762, Chem. Eng. Res. Des. 194 (2023) 136–150, https://doi.org/10.1016/j.cherd.2023 04.029.

[24] M. Assar, H. Asaadian, M. Stanko, B.A. Grimes, A theoretical and experimental investigation of continuous oil– water gravity separation, ISSN 00092509, Chem. Eng. Sci. 298 (2024) 120375, https://doi.org/10.1016/j.ces.2024.120375.

[25] Mehmet Velioglu, Song Zhai, Sophia Rupprecht, Alexander Mitsos, Andreas Jupke, and Manuel Dahmen. Physics-informed neural networks for dynamic process operations with limited physical knowledge and data. Computers & Chemical Engineering. 2024. 108899. doi: 10.1016/j.compchemeng.2024.108899. ISSN 00981354.

[26] S. Song, X. Liu, C. Li, Z. Li, S. Zhang, W. Wei, B. Shi, Q.i. Kang, W. Haihao, J. Gong, Dynamic simulator for three-phase gravity separators in oil production facilities, ACS Omega 8 (6) (2023) 6078–6089, https://doi.org/10.1021/acsomega.2c08267.

[27] A. Uhl, A. Schmidt, M.W. Hlawitschka, J. Strube, Autonomous liquid–liquid extraction operation in biologics manufacturing with aid of a digital twin including process analytical technology, Processes 11 (2) (2023) 553, https://doi.org/10.3390/pr11020553.

[28] M. Soika, A. Pfennig, Extraktion - eine frage des wassers?, ISSN 0009-286X, Chem. Ing. Tech. 77 (7) (2005) 905–911, https://doi.org/10.1002/cite.200500032.

[29] J. Eberz, S. Sibirtsev, A. Jupke, Mini-batch settling cell for investigation of liquid-liquid phase separation, ISSN 00092509, Chem. Eng. Sci. 301 (2025), https://doi.org/10.1016/j.ces.2024.120751.

[30] Joseph Redmon, Santosh Divvala, Ross Girshick, and Ali Farhadi. You only look once: Unified, real-time object detection. In *29th IEEE Conference on Computer Vision and Pattern Recognition*, pages 779– 788, Piscataway, NJ, 2016. IEEE. ISBN 978-1-4673-8851-1. doi: 10.1109/CVPR.2016.91.

[31] G. Jocher, A. Chaurasia, J. Qiu. *Ultralytics YOLOv8*. 2023. URL https://scholar.google.co.uk/citations?user=swsrgtsaaaaj& hl=en&oi=sra.

[32] A. Palmtag, L. Lehmann, L.R. Hanz, U. Kiseleva, A. Jupke, Towards the digital extraction column: Onlinemonitoring and analysis of fluid dynamics in liquid-liquid extraction columns, ISSN 26668211, Chem. Eng. J. Adv. 22 (2025) 100727, https://doi.org/10.1016/j.ceja.2025.100727.

[33] P. Schmitt, M.W. Hlawitschka, H.-J. Bart, Centrifugal pumps as extractors, ISSN 0009-286X, Chem. Ing. Tech. 92 (5) (2020) 589–594, https://doi.org/10.1002/cite.201900105.

[34] Stepan Sibirtsev, Song Zhai, Mathias Neufang, Jakob Seiler, and Andreas Jupke. Mask r-cnn based droplet detection in liquid-liquid systems. part 1: A proof of concept. 2023. 133–139.

[35] S. Sibirtsev, S. Zhai, M. Neufang, J. Seiler, A. Jupke, Mask r-cnn based droplet detection in liquid–liquid systems, part 2: Methodology for determining training and image processing parameter values improving droplet detection accuracy, ISSN 13858947, Chem. Eng. J. 473 (2023), https://doi.org/10.1016/j.cej.2023.144826.

[36] S. Sibirtsev, S. Zhai, A. Jupke, Mask r-cnn based droplet detection in liquid–liquid systems, part 3: Model generalization for accurate processing performance independent of image quality, ISSN 02638762, Chem. Eng. Res. Des. 202 (2024) 161–168, https://doi.org/10.1016/j.cherd.2023.12.005.

[37] H.T. Chen, S. Middleman, Drop size distribution in agitated liquid–liquid systems, ISSN 0001-1541, AIChE J 13 (5) (1967) 989–995, https://doi.org/10.1002/aic.690130529.

[38] A. Mersmann, Zum flutpunkt in flüssig/flüssig– gegenstromkolonnen, ISSN 0009-286X, Chem. Ing. Tech. 52 (12) (1980) 933–942, https://doi.org/10.1002/cite.330521203.

[39] J. Kampwerth, B. Weber, J. Rußkamp, S. Kaminski, A. Jupke, Towards a holistic solvent screening: on the importance of fluid dynamics in a rate-based extraction model, ISSN 00092509, Chem. Eng. Sci. 227 (2020), https://doi.org/10.1016/j.ces.2020.115905.

[40] G.G. Stokes, On the effect of the internal friction of fluids on the motion of pendulums, in: Mathematical and Physical Papers, Cambridge University Press, 2009, pp. 1–10, doi: 10.1017/cbo9780511702266.002.

[41] T. Pilhofer and D. Mewes. Siebboden-Extraktionskolonnen: Vorausberechnung unpulsierter Kolonnen. 1979.

[42] M. Ishii, N. Zuber, Drag coefficient and relative velocity in bubbly, droplet or particulate flows, ISSN 0001-1541, AIChE J 25 (5) (1979) 843–855, https://doi.org/10.1002/aic.690250513.

[43] M. Kraume, A. Gäbler, K. Schulze, Influence of physical properties on drop size distribution of stirred liquid-liquid dispersions, ISSN 0930-7516, Chem. Eng. Technol. 27 (3) (2004) 330–334, https://doi.org/10.1002/ceat.200402006.

[44] S. Sibirtsev, L. Thiel, S. Zhai, Y.T. Cai, L. Recke, A. Jupke, Experimental and model–based investigation of the droplet size distribution during the mixing process in a batch–settling cell, Can. J. Chem. Eng. (2024), https://doi.org/10.1002/cjce.25563. ISSN 00084034.